JOURNAL OF GEOPHYSICAL RESEARCH, VOL. 101, NO. B5, PAGES 11,317–11,327, MAY 10, 1996

Finite element modeling of crustal deformation in the North America–Caribbean plate boundary zone

P. R. Lundgren

Jet Propulsion Laboratory, California Institute of Technology, Pasadena

R. M. Russo[1]

Department of Terrestrial Magnetism, Carnegie Institution of Washington, Washington, D.C.

Abstract. We have developed two-dimensional spherical shell finite element models of elastic displacements in the North America-Caribbean (NA-Ca) plate boundary zone (PBZ) in order to quantify crust and fault motions in the PBZ. The models we derive are dependent on both the internal fault constraints and the NA-Ca Euler pole we used. Since the location and magnitude of the NA-Ca euler pole are still matters of much debate, we consider three Euler poles [*DeMets et al.*, 1990; *Calais and Mercier de Lépinay*, 1993; and *Deng and Sykes*, 1995]. We compare the resulting finite element model displacements to recent seismicity and to geological and geophysical field observations. The model of *DeMets et al.* [1990], NUVEL-1, features an NA-Ca relative velocity across the PBZ which is less than the observed Cayman spreading axis rate, and thus, the finite element model based on it produces fault motions which are inconsistent with observation. The *Calais and Mercier de Lépinay* [1993] (C&M), and *Deng and Sykes* [1995] (D&S) models both yield far-field rates across the PBZ at the point of the Cayman spreading center of approximately 20 mm/yr, a value greater than the observed rate. The greatest differences in the latter two models lie in the motion calculated for the area around Puerto Rico. Both models feature a counterclockwise rotation of the PBZ around Puerto Rico with opening of the Anegada Passage and compression at the Muertos Trough south of eastern Hispaniola. The C&M-based model produces normal opening of the Anegada Passage fault system, while the D&S-based model produces left-lateral transtension across the Anegada Passage fault system, the result of continuum crustal motions which are nearly orthogonal between the two models in the area NE of Puerto Rico. We conclude that the C&M-based model better matches geological observations of PBZ fault motions and deformation primarily on the basis of the Anegada Passage results. Because of this rotation of the PBZ from Hispaniola to the Anegada Passage fault system, the Puerto Rico Trench includes highly oblique compression in its eastern portion, changing to pure left-lateral strike-slip NW of Puerto Rico. The C&M-based finite element model agrees with preliminary GPS results from Hispaniola and Puerto Rico if the central Septentrional fault is constrained to strike-slip motion.

Introduction

We have developed two-dimensional finite element models of the North America-Caribbean (NA-Ca) plate boundary zone (Figure 1) [*Molnar and Sykes*, 1969; *Jordan*, 1975; *Sykes et al.*, 1982; *DeMets et al.*, 1990; *Calais and Mercier de Lépinay*, 1993; *Deng and Sykes*, 1995], and we analyze elastic solutions to assess displacement rates and slip directions on the region's major faults. The models depend on both the relative motion Euler poles for the two plates and on the geometries and constraints of faults within the plate boundary zone. Since there is no definitive solution for the far-field NA-Ca Euler pole location and rate, we must consider a suite of models with the same imposed fault geometries and slip constraints and evaluate the poles by comparison of calculated and observed slip rates and directions on plate boundary zone faults. The models predict distributions of crustal motions throughout the NA-Ca margin, and because they are elastic solutions, we can also compare them directly with observed patterns of recent seismicity. An evaluation of currently used Euler poles of the motions of this plate pair is highly desirable because the location and magnitude of the NA-Ca Euler pole are still matters of debate [*Jordan*, 1975; *MacDonald*, 1976; *Minster and Jordan*, 1978; *Sykes et al.*, 1982; *Stein et al.*, 1988; *DeMets et al.*, 1990; *Calais and Mercier de Lépinay*, 1993; *Deng and Sykes*, 1995]. A strength of our modeling approach is that we can consider a deformable plate boundary zone (PBZ) which accommodates a variety of distributed deformation patterns between two rigid plates. Thus we have quantitative advantages over previous evaluations of far-field NA-Ca rotation models which relied on rigid plate rotations to assess a given model's fit to PBZ geological observations [*Heubeck and Mann*, 1991].

We based our finite element models on three recent studies of NA-Ca relative motion. The global plate motion velocity

[1]Now at Laboratoire de Tectonophysique, Université Montpellier II, Montpellier, France.

Paper number 95JB03747.
0148-0227/96/95JB-03747$09.00

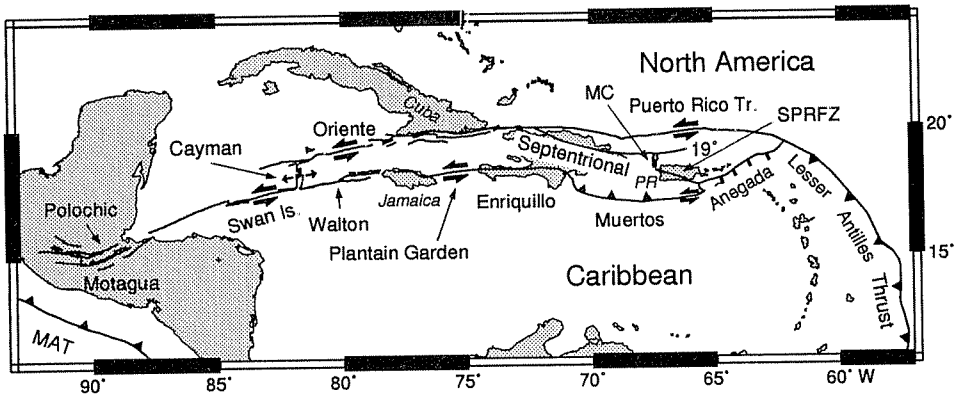

Figure 1. Tectonic map of the North America-Caribbean plate boundary zone. Major faults described in the text are indicated, with the following abbreviated: MAT, Middle America Trench; MC, Mona Canyon; SPRFZ, Southern Puerto Rico fault zone. *PR*, Puerto Rico.

model, NUVEL-1, of *DeMets et al.* [1990] is a "classical" kinematic model obtained by inversion of available spreading rates, transform fault and earthquake slip vector azimuths for an ensemble of plate pairs, yielding a minimum summed error solution for all plate pairs. NUVEL-1 is based on the assumption that the transform faults bounding the Cayman spreading center are pure strike-slip faults representative of instantaneous NA-Ca motion. Although *DeMets et al.* [1990] used a Cayman spreading rate derived from magnetic anomalies of 15 mm/yr (based on *Rosencrantz et al.* [1988]) in their inversion, velocity closure requirements predict only 12 mm/yr NA-Ca relative motion at the Cayman spreading axis. *Deng and Sykes* [1995] (D&S) used a least squares method to compute an NA-Ca Euler pole from NA-Ca PBZ earthquake slip vectors and then calculated an angular rotation rate such that it produces 20 mm/yr relative motion at the Cayman spreading center. They proposed that the mean rate derived from Cayman Trough spreading underestimates the full plate motion because of past or current slip along presumed Cayman fracture zones, and that motion directions based on Cayman transform faults may be unreliable if deformation has modified their azimuths [*Sykes et al.*, 1982]. Thus NUVEL-1 accounts for no distributed deformation in the plate boundary, whereas the D&S model requires such distributed shear to accommodate high far-field rates. The third model we consider is that of *Calais and Mercier de Lépinay* [1993], who calculated the surface strain of a given plate boundary fault segment based on its obliquity to a suite of trial Euler poles. They then compared these surface strains with a model of surface strain along the plate boundary derived from geologic observations and chose a best fit Euler pole from a grid of trial poles. The magnitude of their Euler vector is calculated to give an NA-Ca relative rate of 20 mm/yr at the Cayman spreading axis. The Swan Islands and western Oriente faults lie on small circles about the NA-Ca Euler poles for all three models. However, differences in Euler pole locations predict differences in relative motion across the eastern portion of the plate boundary zone. Thus the models compare the various Euler poles predictions primarily for eastern plate boundary deformation. The goal of this paper, however, is not to provide a definitive resolution of the NA-Ca Euler pole parameters, but instead to derive a model for continuum and fault motion throughout the NA-Ca PBZ.

The North America-Caribbean Plate Boundary Zone

We describe briefly the major faults of the NA-Ca plate boundary zone (Figure 1). The westernmost portion of the NA-Ca plate boundary zone is exposed onland in Central America as the complexly deformed left-lateral Motagua-Polochic fault system [*Langer and Bollinger*, 1979; *Guzman-Speziale et al.*, 1989], which connects offshore to the Swan Islands fault. Recent marine geophysical studies have shown that the Swan Islands fault is a sharply defined pure strike-slip fault along much of its trace, with the exception of one small region of overstepping splays [*Rosencrantz and Mann*, 1991; *Mann et al.*, 1991]. Seismicity along the fault (Figure 2) clearly indicates pure left-lateral slip. We infer from the simplicity of Swan Islands fault structures and seismicity that the fault is the plate boundary and that motion here is not distributed across a wide zone as it is further east. The Swan Islands fault terminates eastward at the southern end of the Cayman spreading center, which has normal faulting earthquakes (Figure 2) and generates the magnetic anomalies of the Cayman Trough [*Rosencrantz et al.*, 1988]. The northern end of the Cayman spreading axis terminates against the Oriente fault, characterized by pure left-lateral strike-slip motions in its portion west of Cuba (Figure 2). Oriente fault structures are increasingly complex south of Cuba, where they include folds and thrust faults [*Calais and Mercier de Lépinay*, 1991], and in eastern Hispaniola, where several splays are active in a restraining bend [*Mann et al.*, 1984; *Russo and Villaseñor*, 1995]. In particular, the Septentrional fault, the principal displacement surface of the Hispaniola restraining bend, has been the locus of very large magnitude mixed thrust and strike-slip earthquakes in recent times [*Prentice et al.*, 1993; *Russo and Villaseñor*, 1995]. South of the Oriente fault, the southern edge of the plate boundary zone is defined by the left-lateral strike-slip Walton fault from the southeast end of the Cayman spreading axis through Jamaica, where it is known as the Plantain Garden fault, to the Enriquillo fault, coincident with Haiti's southern peninsula [*Burke et al.*, 1980; *Mann et al.*, 1984; *Rosencrantz and Mann*, 1991]. Between the eastern end of the Enriquillo fault in southern Hispaniola and the western portion of the Septentrional fault lies a zone of NW-SE trending thrust

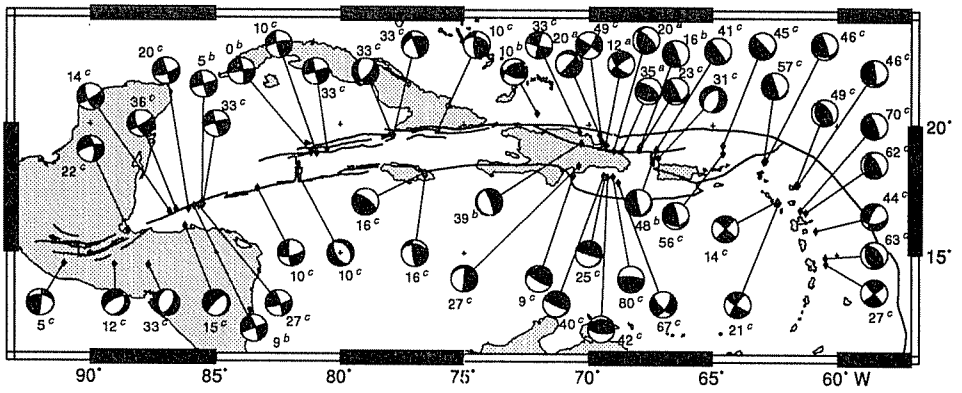

Figure 2. Earthquake focal mechanisms for selected earthquakes in the northern Caribbean region. Large number adjacent focal mechanism is its depth, superscript is its reference source: *a, Russo and Villaseñor* [1995]; *b, Molnar and Sykes* [1969]; *c,* Harvard centroid-moment tensor solutions 1977-1993 (see *Dziewonski et al.* [1981], for description).

faults, including the San Juan-Los Pozos fault zone, which bounds the SW extent of thrusting [*Mann et al.,* 1995].

From Hispaniola eastward, the number and complexity of plate boundary zone structures increase again. The northern NA-Ca plate boundary includes both the Puerto Rico Trench, with active left-lateral strike-slip and normal faults [*Molnar,* 1977; *Masson and Scanlon,* 1991; *Speed and Larue,* 1991], and the 19 Degree fault, which also has normal displacement [*Speed and Larue,* 1991]. The 19 Degree fault intersects the seismically active Mona Canyon graben [*Speed and Larue,* 1991; *Masson and Scanlon,* 1991]. The southern reaches of the NA-Ca plate boundary zone here are defined by the bathymetric Muertos Trough, which is associated with sediments deformed in a compressional tectonic environment [*Ladd et al.,* 1977, 1981; *Ladd and Watkins,* 1978] and earthquakes indicative of active underthrusting of Caribbean lithosphere beneath terranes including eastern Hispaniola and Puerto Rico [*Byrne et al.,* 1985; *McCann and Pennington,* 1990; *Masson and Scanlon,* 1991]. South of Puerto Rico there is evidence that Muertos Trough convergence decreases eastwards [*Masson and Scanlon,* 1991] with strike-slip motion (P. Jansma, personal communication, 1995) near its intersection with the confluence of the Southern Puerto Rico fault system and the Anegada Passage fault system. The Anegada Passage fault system cuts diagonally across the plate boundary zone and is the locus of normal faulting and/or transtension [*Jany et al.,* 1990]. The Puerto Rico Trench is morphologically continuous with the northeastern Lesser Antilles thrust, an active subduction zone defined by seismicity to depths of 200 km [*Molnar and Sykes,* 1969; *Tomblin,* 1975; *Stein et al.,* 1982; *Sykes et al.,* 1982].

Several authors have proposed that distinct crustal blocks exist in the eastern NA-Ca plate boundary zone. The eastern Cayman Trough region between the Walton and Oriente faults, extending into western Hispaniola, has been named the Gonave Microplate by *Rosencrantz and Mann* [1991]. A sliver of the northeast coast of Hispaniola, including the Cordillera Septentrional and the Samaná Peninsula, is in motion relative to the rest of the island [*Mann et al.,* 1984; *Russo and Villaseñor,* 1995]. The area of Puerto Rico and the Virgin Islands bounded by the Mona Canyon, 19 Degree fault, Anegada Passage faults, and the Muertos Trough has also been identified as a coherent block [*Byrne et al.,* 1985; *Jany et al.,* 1990; *Masson and Scanlon,* 1991]. This area has been interpreted either as a counter-clockwise rotating microplate [*Masson and Scanlon,* 1991] or a tectonically escaping block [*Jany et al.,* 1990]. The finite element method is potentially useful in testing some of these hypotheses because it can account for complex deformation patterns, both as displacements on faults and continuum strain, without imposing rigid block behavior.

Method

We use a finite element formalism which includes geologic constraints to model the kinematics and deformation of the NA-Ca plate boundary zone [*Saucier and Humphreys,* 1993; *Lundgren et al.,* 1995]. The finite element solution for a linear elastic problem is expressed in the form of a weighted least squares equation [*Saucier and Humphreys,* 1993]. The solution minimizes the strain energy in the plate and provides estimates for block deformation, motion, and fault slip rates everywhere in the finite element array. A Monte Carlo technique is used to interpret the sensitivity and uncertainties in the model due to complexities in the data. For our application to the northern Caribbean region, we solve for nodal displacements on an elastic, two-dimensional (2-D) spherical shell with a plane stress condition ($\sigma_3 = 0$). We use eight-node, biquadratic, isoparametric elements.

The crustal layer is modeled as a two-dimensional elastic plate, cut by active faults. Faults are surfaces in which (1) only the slip direction is constrained; (2) both the slip direction and rate are known; or (3) both the direction and rate are unconstrained. Fault slip data are implemented as described by *Melosh and Raefsky* [1981], and introduce torque-free dislocations in the continuum. Fault orientations are prescribed as free-shear surfaces [*Melosh and Williams,* 1989].

Far-field displacements are imposed as boundary conditions. For a spherical geometry, relative plate motions imposed at the mesh boundary are calculated on the basis of a given boundary node's angular distance from the Euler pole. Likewise, the overall orientation of the finite element mesh boundaries is controlled by the Euler pole location, since we choose to have the boundaries fall on either great or small circles relative to the rotation pole. Thus, when we compare models based on different poles, the locations of the mesh boundaries reflect differences in pole location.

The most significant difference between this approach and

the rigid plate model of *Chase* [1972], and its applications to the *n*-plate problem by *Minster and Jordan* [1978] and *DeMets et al.* [1990], is that we include deformable blocks. Unlike the rigid plate inversion, local misfits between observed and predicted motions are "absorbed" locally, rather than being spread equally at all boundary locations of adjacent plates. Spatially close parameters are more highly correlated than distant ones, yet the overall solution is that which is closest to the rigid plate model.

In the finite element approximation the displacements $\mathbf{u}(x,y) = \mathbf{u}^e = \mathbf{N}^e \boldsymbol{\zeta}^e$ are calculated from the nodal displacements for the element $\boldsymbol{\zeta}^e$ through the matrix of interpolation functions $\mathbf{N}^e$ [*Zienkiewicz and Taylor*, 1989]. For Hooke's material with no residual stresses ($\sigma_0 = 0$) and no initial strains ($\varepsilon_0 = 0$), the constitutive property for a linear isotropic elastic medium is

$$\boldsymbol{\sigma} = \mathbf{D}\boldsymbol{\varepsilon} \tag{1}$$

where $\mathbf{D}$ is a matrix containing Lamé's coefficients in the plane stress approximation. Thus the strain on a spherical shell is

$$\boldsymbol{\varepsilon} = \begin{pmatrix} \varepsilon_\theta \\ \varepsilon_\phi \\ 2\varepsilon_{\theta\phi} \end{pmatrix} =$$

$$\frac{1}{R}\left\{\begin{bmatrix} \frac{\partial}{\partial\theta} & 0 \\ 0 & \frac{1}{\sin\theta}\frac{\partial}{\partial\phi} \\ \frac{1}{\sin\theta}\frac{\partial}{\partial\phi} & \frac{\partial}{\partial\theta} \end{bmatrix} + \begin{bmatrix} 0 & 0 \\ \cot\theta & 0 \\ 0 & -\cot\theta \end{bmatrix}\right\}\begin{pmatrix} u_\theta \\ u_\phi \end{pmatrix} =$$

$$\mathbf{Su} = \mathbf{SN}\boldsymbol{\zeta} = \mathbf{B}\boldsymbol{\zeta} \tag{2}$$

where (θ, ϕ) are the colatitude and longitude, respectively, and R is the radius of the shell (radius of the earth). For an elastic body in equilibrium, we use a variational principle to solve for the minimum in the potential energy with respect to small nodal displacements. For a given element, e, the elastic strain energy is

$$U^e = \frac{1}{2}\int_{\Omega^e} \boldsymbol{\varepsilon}^{\mathrm{T}}\boldsymbol{\sigma}\, d\Omega \tag{3}$$

and using Hooke's law (1),

$$U^e = \frac{1}{2}\int_{\Omega^e} \boldsymbol{\varepsilon}^{\mathrm{T}}\mathbf{D}\boldsymbol{\varepsilon}\, d\Omega = \frac{1}{2}\int_{\Omega^e} \boldsymbol{\zeta}^{e\,\mathrm{T}}\mathbf{B}^{e\,\mathrm{T}}\mathbf{D}^e\mathbf{B}^e\boldsymbol{\zeta}^e\, d\Omega \tag{4}$$

where Ω^e is the element volume. For a boundary traction vector $\mathbf{t}$ applied on the boundary of the element, the potential energy of the applied boundary stress is

$$U^e = -\int_S \mathbf{u}^{\mathrm{T}}\mathbf{t}\, dS = -\int_S \left[\mathbf{N}^e\boldsymbol{\zeta}^e\right]^{\mathrm{T}}\mathbf{t}\, dS \tag{5}$$

where S is the surface of the element. Summing (4) and (5) and minimizing the total energy of the body under load with respect to small variations in ζ_i, we get the standard finite element equation

$$\mathbf{K}\boldsymbol{\zeta} = \mathbf{f} \tag{6}$$

where

$$\mathbf{K}^e = \int_{\Omega^e} \mathbf{B}^{e\,\mathrm{T}}\mathbf{D}^e\mathbf{B}^e\, d\Omega \tag{7}$$

defines the element stiffness matrix and

$$\mathbf{f}^e = \int_S \mathbf{N}^{e\,\mathrm{T}}\mathbf{t}\, dS \tag{8}$$

defines the element force vector. The global stiffness matrix $\mathbf{K}$ is assembled from $\mathbf{K}^e$ and is solved for by Gaussian integration. Displacement boundary conditions and fault slip data (split nodes) enter into (8) which reduces the rank to the number of degrees of freedom. A sufficient condition for $\mathbf{K}$ to be inverted is that the translation and rotation for each element are constrained so the solution $\boldsymbol{\zeta} = \mathbf{K}^{-1}\mathbf{f}$ exists.

We calculate uncertainties in the model predictions via a Monte Carlo method to construct the probability distribution for the deformation everywhere. This is computationally efficient since the kinematic data enter the model in the force vector $\mathbf{f}$, so the stiffness matrix $\mathbf{K}$ is inverted only once. Histograms are constructed from typically 1000 computational runs, allowing the standard deviation to be calculated.

Models and Constraints

We create finite element models whose mesh orientation and far-field plate rates are based on three determinations of the NA-Ca rotation pole [*DeMets et al.*, 1990; *Calais and Mercier de Lépinay*, 1993 (C&M); *Deng and Sykes*, 1995]. In our models we use the following material properties: Youngs modulus, 7×10^{10} Pa; Poisson's ratio, 0.25; which enter into the $\mathbf{D}$ matrix in equation (1) [see *Zienkiewicz and Taylor*, 1989]. In defining the faults in the mesh, we left fault slip unconstrained except when slip direction and/or magnitude are known from geologic or seismic evidence. We prescribed the Cayman spreading center to normal spreading at a rate of 16 mm/yr [*Rosencrantz et al.*, 1988]. We required normal convergence at the full NA-Ca relative motion rate along the Lesser Antilles thrust. The Walton and Plantain Garden-Enriquillo faults are modeled as strike-slip faults, as indicated by marine geophysical and field data [*Burke et al.*, 1980; *Mann et al.*, 1984, 1995; *Rosencrantz and Mann*, 1991]. We model the Muertos Trough with normal convergence in its western portion (Figure 2), and left-lateral strike-slip motion along its easternmost portion (P. Jansma, personal communication, 1995).

Figures 3, 4, and 5 show the finite element meshes for the NUVEL-1-based, D&S-based, and C&M-based models, respectively. Each mesh is based on an oblique Mercator projection about the Euler pole, but shown in the figures on a Mercator projection about the Earth's spin axis. In these plots the long, sublatitudinal northern boundary of the mesh is a small circle about the NA-Ca relative rotation pole, and are lines of constant relative motion. Variations in the relative rate along the sublongitudinal eastern and western boundaries of the meshes are proportional to $\sin\theta$, where θ are the colatitudes from the Euler pole. All models have the same boundary conditions and fault constraints: free-slip along the top and bottom of the NA plate; right and left sides of the NA plate rotate at the rate prescribed by their distance from the pole; left and bottom sides of the Caribbean plate are fixed.

Discussion

The NUVEL-1-based model (where mesh orientation and far-field boundary rates are based on the NUVEL-1 model of *DeMets et al.* [1990]; see Figure 3) is the only model which clearly does not fit the observed left-lateral motion along the

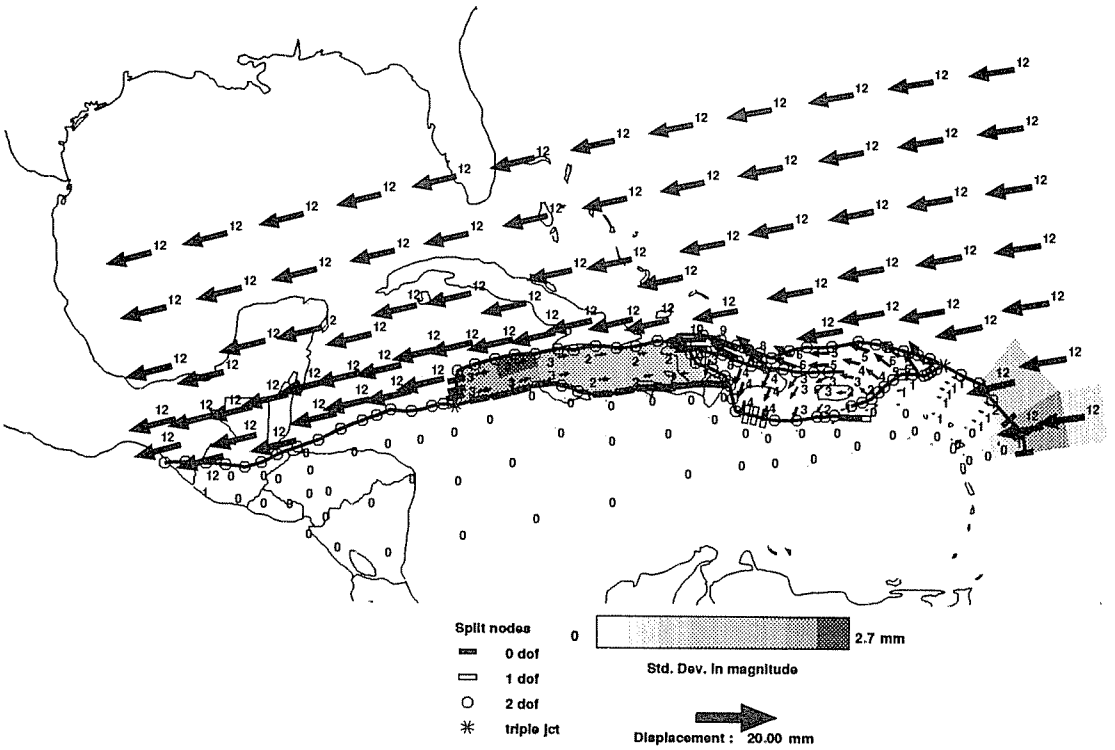

Figure 3a. NUVEL-1 [*DeMets et al.*, 1990] based model: finite element solution plotted on a Mercator projection in geographic coordinates. Solid arrows show the calculated motions at the center of each element with its length proportional to its magnitude, with the magnitude value printed next to each arrow. The mesh is plotted as a Mercator projection in geographic coordinates. Also shown are the model fault node constraints: 0 degrees of freedom (dof), split node constrained in direction and magnitude; 1 dof, free slip fault node constrained parallel to a prescribed direction only; 2 dof, unconstrained fault node. The shading of each element shows the standard deviation in rate for each element after 1000 Monte Carlo runs.

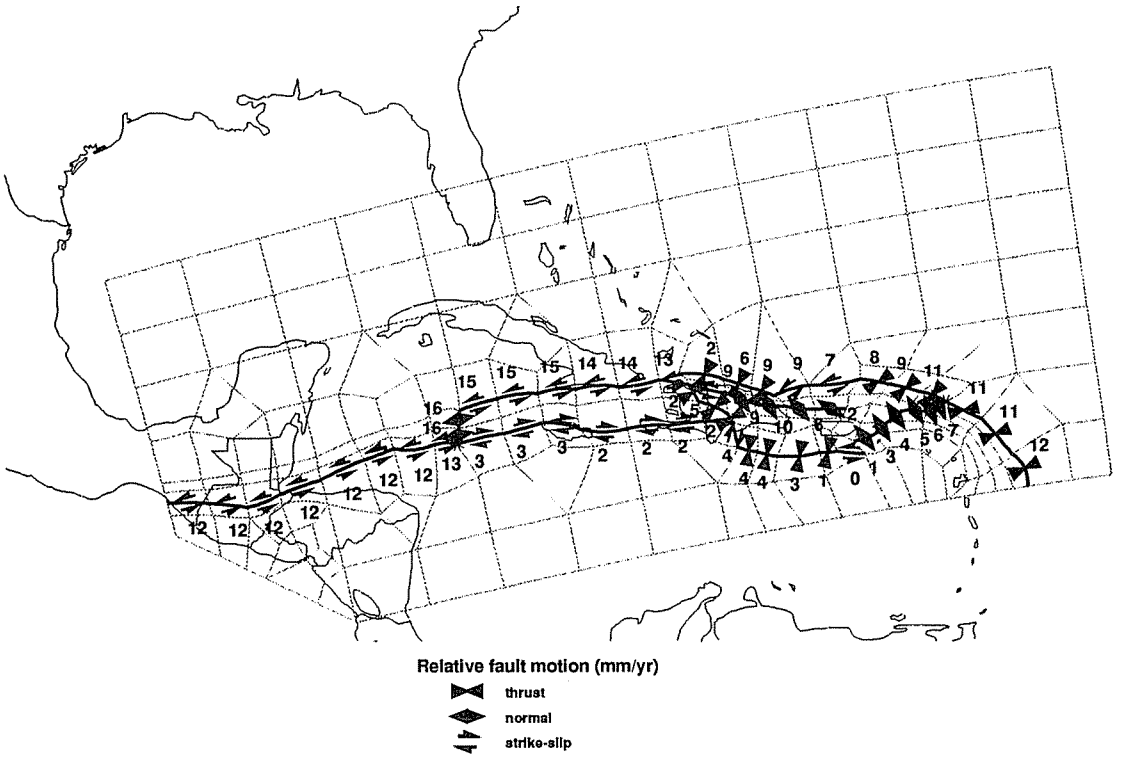

Figure 3b. NUVEL-1 [*DeMets et al.*, 1990] based model: fault rate solution showing the magnitude and sense of motion at fault nodes lying at the middle of element sides.

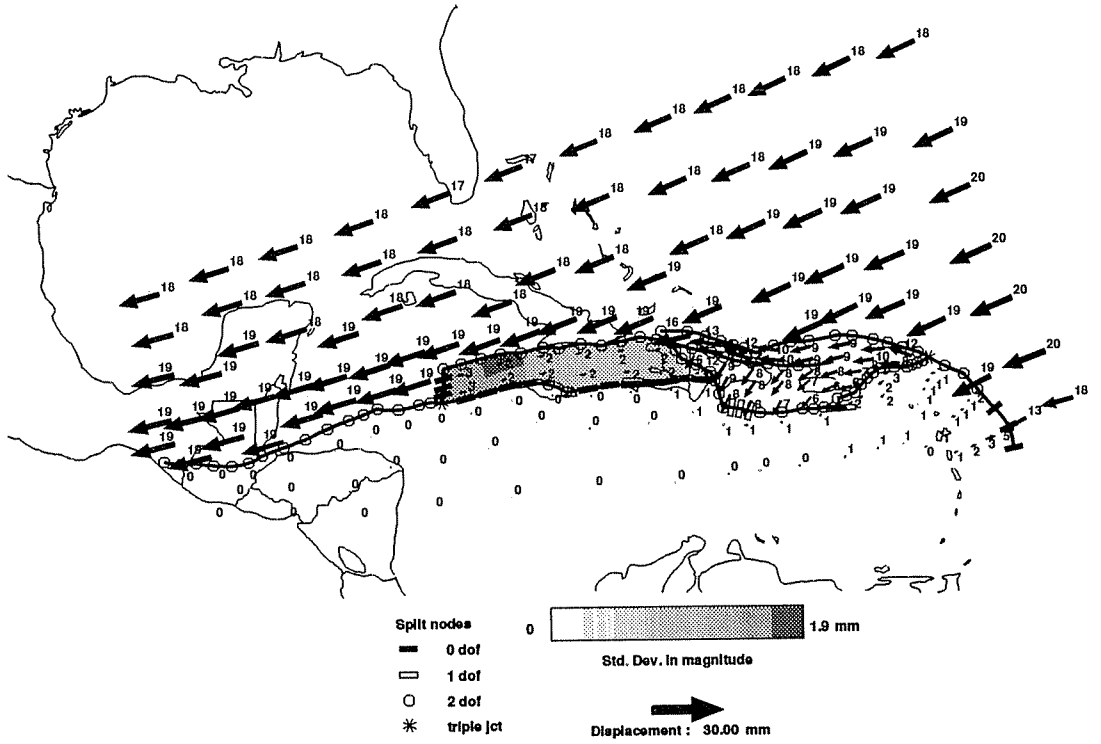

Figure 4a. *Deng and Sykes* [1995] based model: calculated motions at the center of each element (see Figure 3a for explanation).

Walton-Plantain Garden-Enriquillo fault system [*Mann et al.*, 1995] and the observed compression at the Jamaica restraining bend (*Burke et al.* [1980]; Fig. 2 focal mechanism). This is not unexpected given that its far-field NA-Ca rate is less than the observed Cayman spreading rate. Despite this, we note how similar the NUVEL-1-derived motion patterns are in the eastern PBZ when compared to the results of the other two models. This illustrates how localized the effects of fault constraints are in the finite element solution.

Displacements calculated from both the C&M and D&S Euler poles reproduce the major observed characteristics of the NA-Ca plate boundary zone (Figures 4 and 5). Each model

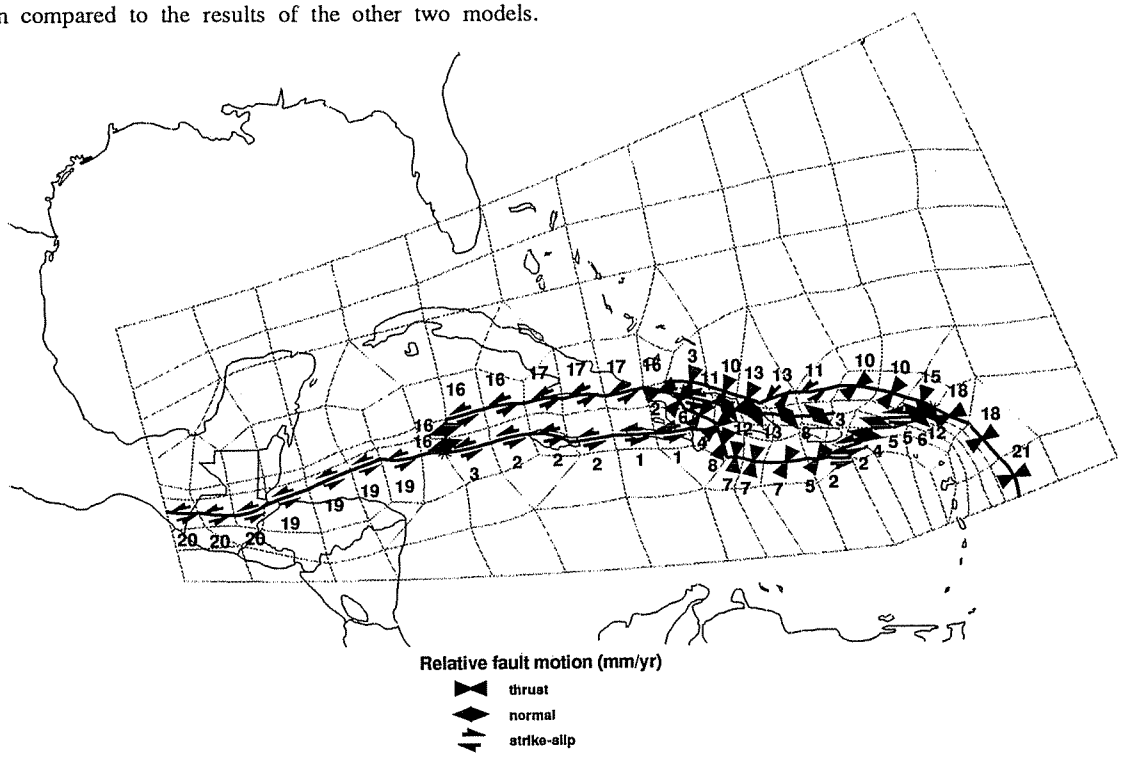

Figure 4b. *Deng and Sykes* [1995] based model: fault rate solution (see Figure 3b for explanation).

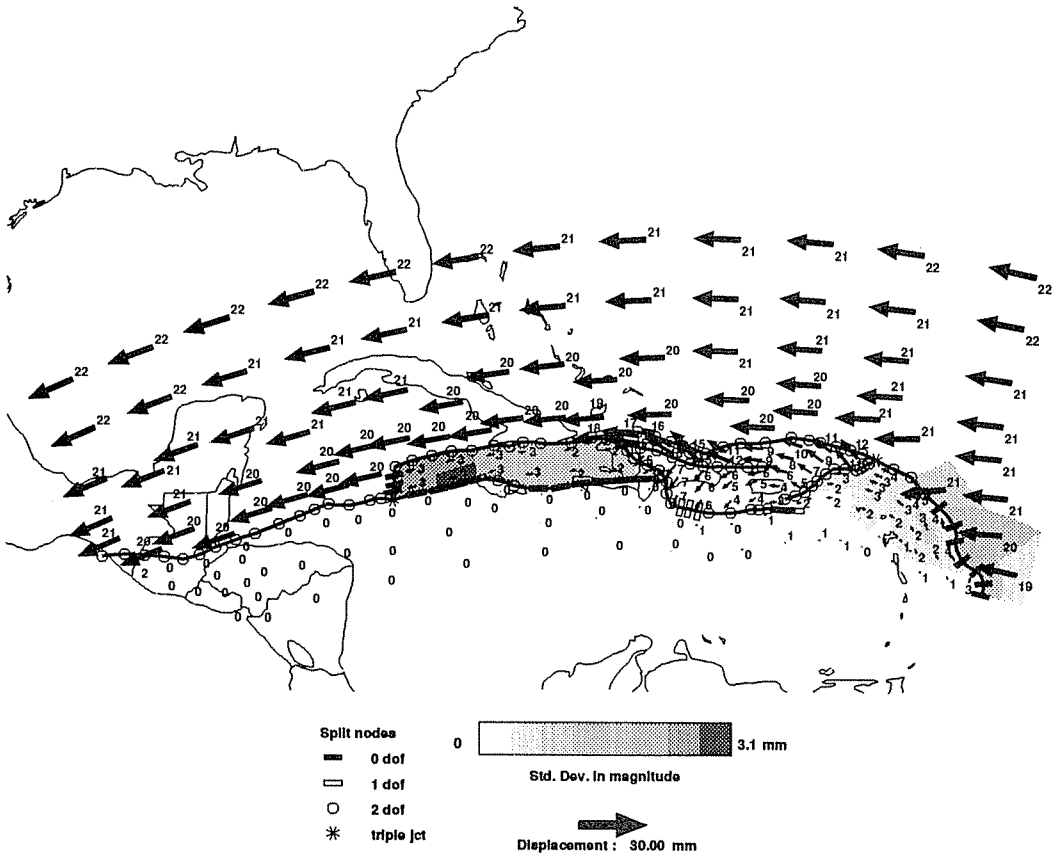

Figure 5a. *Calais and Mercier de Lépinay* [1993] based model: calculated motions at the center of each element (see Figure 3a for explanation).

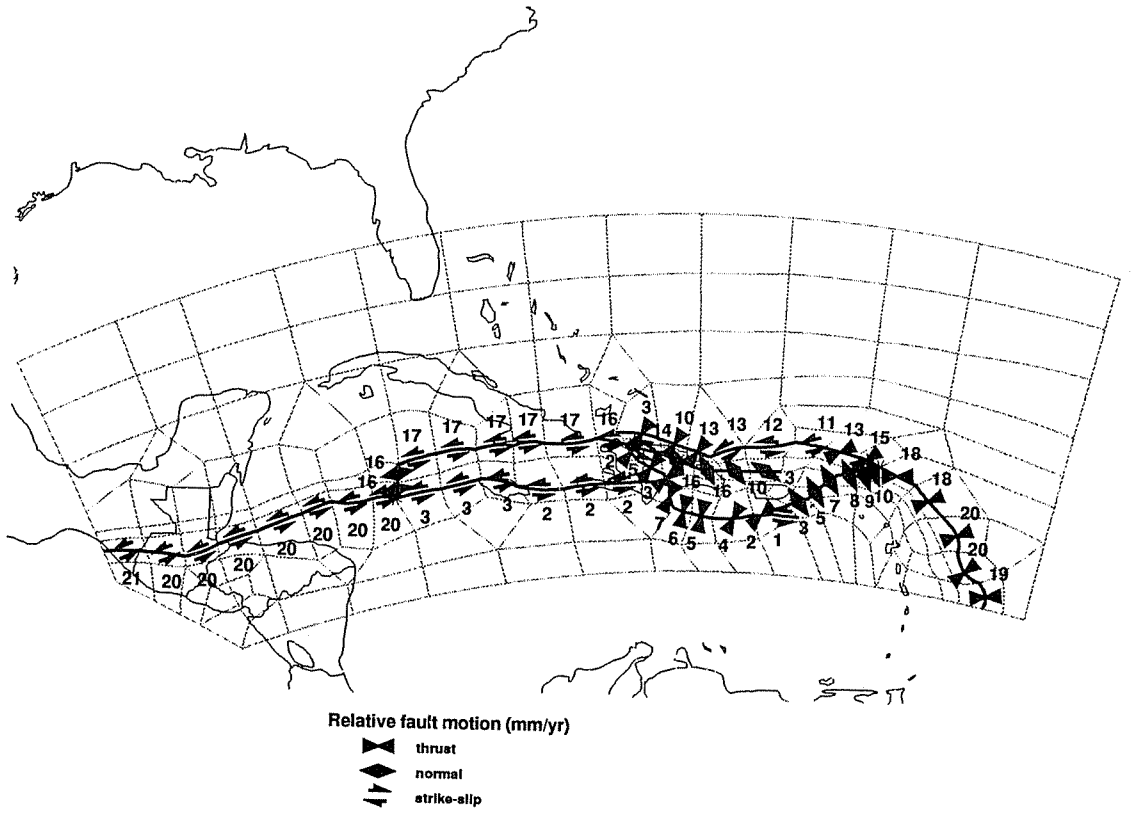

Figure 5b. *Calais and Mercier de Lépinay* [1993] based model: fault rate solution (see Figure 3b for explanation).

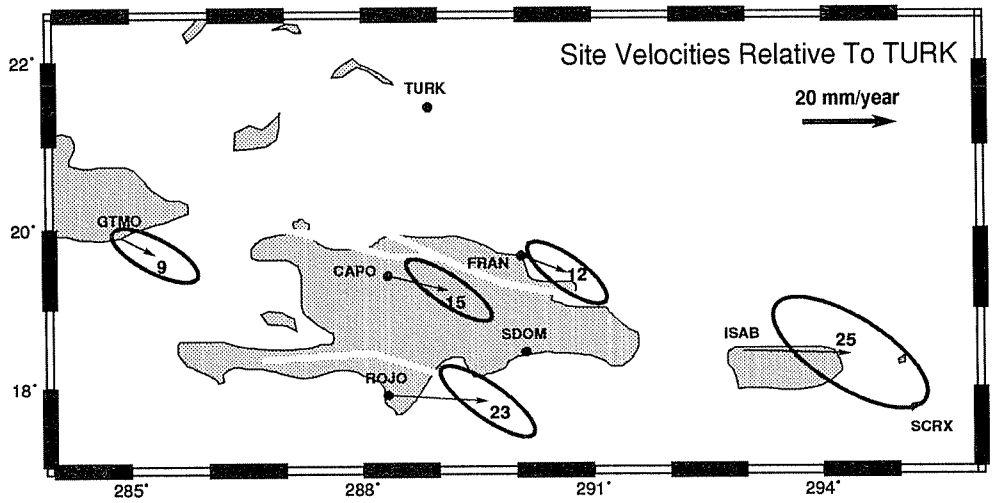

Figure 6. Preliminary GPS site velocity vectors and their 95% confidence ellipses with respect to site TURK in the Bahamas on stable North America plate for two occupations in 1986 and 1994 from *Farina et al.* [1995].

produces left-lateral strike-slip motion along the Swan Islands fault system and at the western ends of the Oriente and Walton faults, where these faults intersect the Cayman spreading center. In fact, the two models predict low-velocity left-lateral strike-slip displacements (1-3 mm/yr) on the Walton-Plantain Garden-Enriquillo fault system. Motions in the vicinity of Jamaica are clearly transpressive in the restraining bend of this fault system. Along the Puerto Rico Trench, displacements evolve from highly oblique compression east of Puerto Rico to increasing strike-slip north and west of the island. In these models, we have left the motion on both the Septentrional and the offshore continuation of the Puerto Rico trench fault system northeast of Hispaniola unconstrained; the Septentrional evolves from transtension at the 19 Degree fault to transpression at its western end, but the offshore Hispaniola fault system is predominantly thrust. Western Hispaniola is undergoing active compression as evidenced by anticlinal mountains and uplifting coral reefs, while eastern Hispaniola shows no uplift [*Mann et al.*, 1995]. At the western end of the offshore Hispaniola fault system north of Haiti there is evidence for predominantly compressive structures [*Dillon et al.*, 1992]. What the exact partitioning of motion is between these two faults is not clear from geologic studies. The along-strike evolution of slip along the Septentrional fault predicted by our models is consistent with the gross sense of coastal uplift in the west and no uplift in eastern Hispaniola. Inclusion in the mesh of the San Juan-Los Pozos fault, striking NW-SE from the western Septentrional to the eastern Enriquillo fault, in central Hispaniola gives slow thrust motion from 1-4 mm/yr along its length, consistent with field observations [*Mann et al.*, 1995].

The C&M-based and D&S-based models differ most significantly in the easternmost PBZ between Puerto Rico and the Anegada Passage fault system. Morphology, bathymetry, and seismicity indicate that the Anegada Passage fault system is an actively extending graben [*Murphy and McCann*, 1979; *Frankel et al.*, 1980; *Jany et al.*, 1990; *Masson and Scanlon*, 1991; *Speed and Larue*, 1991]. The Anegada Passage extension direction is not well constrained by earthquake focal mechanisms; however, evidence for a right-lateral component along the fault system has been proposed based on bathymetry and seismic reflection profiles [*Jany et al.*, 1990]. Northwest of the Anegada Passage, the C&M-based model yields northwest directed crustal motions and strongly normal displacements across the Anegada Passage fault system. The middle portion of the Anegada Passage fault system (the Anegada Passage proper) has a slight right-lateral component to it, in keeping with the marine geophysical evidence of *Jany et al.* [1990], and similar to the block rotation model for the PBZ around Puerto Rico of *Masson and Scanlon* [1991]. In contrast, the D&S-based model gives WSW crustal motions with strongly left-lateral transtensional displacements across the Anegada Passage fault system. In both models the slip rate across the Anegada Passage fault system decreases greatly from NE to SW; at its termination near the eastern end of the Muertos Trough, both models indicate increasing degrees of compression. The latter is not surprising given the fault slip direction constraints of strike-parallel and strike-normal motion across the eastern and western Muertos Trough, respectively, based on earthquake focal mechanism slip directions.

Preliminary Global Positioning System (GPS) results have been determined between several sites in Cuba, Hispaniola, and Puerto Rico with respect to Grand Turk Island in the southern Bahamas (Figure 6) [*Farina et al.*, 1995]. We briefly compare these motion estimates with our C&M-based model results. Figure 7 shows the C&M-based model continuum velocities with North America fixed. Given the large uncertainties in the GPS solutions, the agreement between the C&M-based model and the GPS is quite good. The only major discrepancy we observe between the GPS-derived velocities and our calculations is in the coastal sliver of NE Hispaniola, where our continuum velocities are directed to the NE and the GPS site FRAN has ESE directed motion. If we impose pure strike-slip motion on the central portion of the Septentrional fault, we find a solution (Figure 8) in which the crustal motion at FRAN is ESE-directed. This transfers a tensional component on the SE Septentrional fault system to faults off the NE coast of Hispaniola, resulting in left-lateral strike-slip motion on both fault systems. While faulting NE of Hispaniola is often considered to have a significant compressional component, large-magnitude, left-lateral strike-slip events like the August 8, 1946

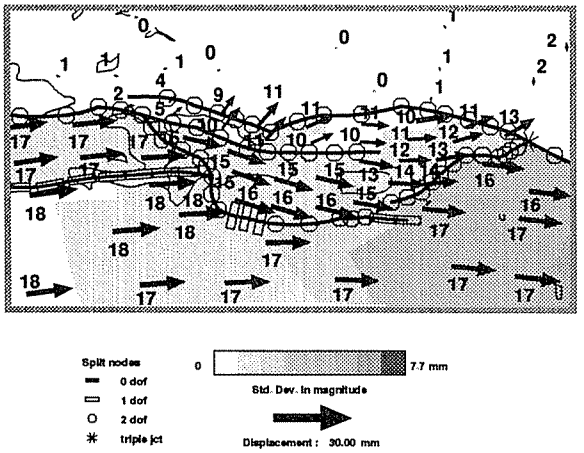

Figure 7. *Calais and Mercier de Lépinay* [1993] based model (inset of Puerto Rico area): calculated motions at the center of each element (see Figure 3a for explanation). This is the same solution as Figure 5a but with the North America plate held fixed so that the continuum velocity vectors can be compared to Figure 6.

event which occurred offshore NE Hispaniola [*Russo and Villaseñor*, 1995], and the overall lack of significant uplift in eastern Hispaniola over the last 125 Ka [*Mann et al.*, 1995] are consistent with the solution shown in Figure 8. Evidence for a component of crustal shortening along the eastern Septentrional fault as revealed by large earthquakes in 1946 [*Russo and Villaseñor*, 1995] are inconsistent with both solutions (Figures 7 and 8) and may reflect the limitations of our two-dimensional modeling of an area of the PBZ that exhibits both vertical and horizontal strain partitioning in the restraining bend.

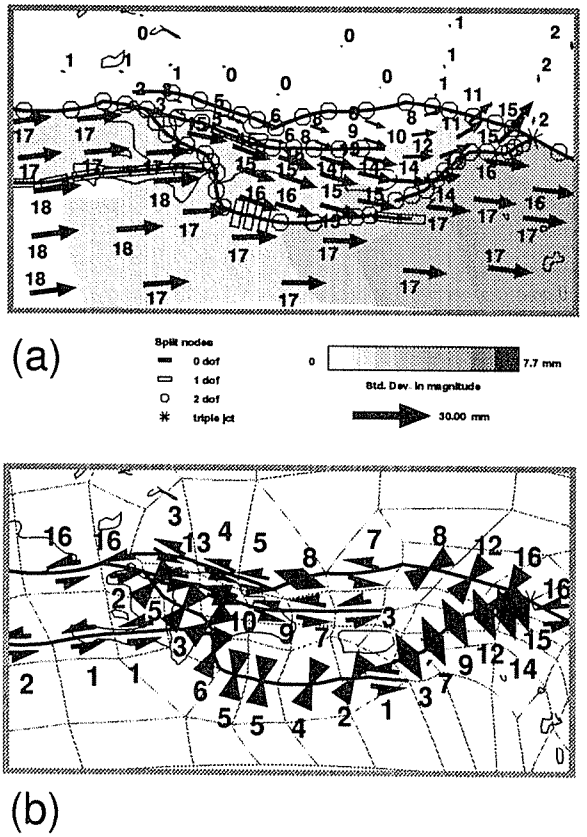

Figure 8. *Calais and Mercier de Lépinay* [1993] based model (inset of Puerto Rico area): (a) calculated motions at the center of each element (see Figure 3a for explanation). This is the same as Figure 7 but with the added constraint that the central Septentrional fault be strike-slip. This produces continuum motions more consistent with the GPS results shown in Figure 6. (b) Fault rate solution (see Figure 3b for explanation).

Conclusions

We formulated three finite element models of displacements in the NA-Ca plate boundary zone based on the most recent relative motion models [*DeMets et al.*, 1990; *Calais and Mercier de Lépinay*, 1993; *Deng and Sykes*, 1995]. The NUVEL-1 model produces relative motions on the Walton-Plantain Garden-Enriquillo faults on the southern side of the plate boundary zone which are inconsistent with their observed sense of motion. Both the *Calais and Mercier de Lépinay* [1993] and *Deng and Sykes* [1995] based finite element models produce rates and patterns of motion which, though different in their continuum motions in the far field, are very similar across most of the major faults in the PBZ. These two models differ most significantly to the east of Puerto Rico and at the Anegada Passage fault zone. Here, the C&M-based model produces normal motion with a slight component of right-lateral slip along the Anegada Passage itself, consistent with marine geophysical data [*Jany et al.*, 1990]. By contrast, the D&S-based model produces left-lateral transtension. Based on these differences, we conclude that a Euler pole such as that of *Calais and Mercier de Lépinay* [1993], which features more strike-parallel relative plate motions along the eastern PBZ yields fault motions in better agreement with observations. Our displacements based on C&M indicate that the Puerto Rico Trench includes highly oblique compression in its eastern portion, changing to pure left-lateral strike-slip north of Puerto Rico. The region around Puerto Rico rotates counterclockwise with N-S extension along the Anegada Passage fault system. The finite element models indicate that NA-Ca relative motion is partitioned as displacement along faults and as continuum deformation (including rotation) throughout the NA-Ca plate boundary zone. Our results are in good agreement with preliminary GPS results [*Farina et al.*, 1995], if we constrain the central Septentrional fault to left-lateral strike-slip motion.

Acknowledgments. We thank Pam Jansma for generously sending us unpublished data and for helpful discussions. We thank C. DeMets, F. Farina, T. Dixon, P. Mann, P. Jansma, and E. Calais for preliminary GPS solutions. Bob Speed read and helped correct flaws in an early version of this work. We thank Eric Calais, Chuck DeMets, and Paul Mann for critical reviews of the manuscript. Bill McCann offered useful advice. Craig Bina provided stimulating conversation and deep insight into folding and crack phenomena in both hydrothermal and glacial environments. We thank Guilhem Barruol for use of computer facilities and logistical help. A research associateship at the Department of Terrestrial Magnetism and NSF grant EAR 93-16457 to P. Silver and R. Russo supported R. Russo during this work. Support for P. Lundgren was provided by the Jet Propulsion Laboratory, California Institute of Technology, under contract to the National Aeronautics and Space Administration.

References

Burke, K., J. Grippi, and A. M. C. Şengör, Neogene structures in Jamaica and the tectonic style of the northern Caribbean plate boundary zone, *J. Geol., 88*, 375-386, 1980.

Byrne, D. B., G. Suarez, and W. R. McCann, Muertos Trough subduction–Microplate tectonics in the northern Caribbean?, *Nature, 317*, 420–421, 1985.

Calais, E., and B. Mercier de Lépinay, From transtension to transpression along the northern Caribbean plate boundary off Cuba: Implications for the recent motion of the Caribbean plate, *Tectonophysics, 186*, 329-350, 1991.

Calais, E., and B. Mercier de Lépinay, Semiquantitative modeling of strain and kinematics along the Caribbean/North America strike-slip plate boundary zone, *J. Geophys. Res., 98*, 8293-8308, 1993.

Chase, C.G., The *n*-plate problem of plate tectonics, *Geophys. J. R. Astron. Soc., 29*, 117-122, 1972.

DeMets, C., R. G. Gordon, D. F. Argus, and S. Stein, Current Plate Motions, *Geophys. J. Int., 101*, 425–478, 1990.

Deng, J., and L. R. Sykes, Determination of Euler pole for contemporary relative motion of Caribbean and North American plates using slip vectors of interplate earthquakes, *Tectonics, 14*, 39-53, 1995.

Dillon, W. P., J. A. Austin, K. M. Scanlon, N. T. Edgar, and L. M. Parson, Accretionary margin of north-western Hispaniola: Morphology, structure and development of the northern Caribbean plate boundary, *Mar. Pet. Geol., 9*, 70-88, 1992.

Dziewonski, A. M., T. -A. Chou, and J. H. Woodhouse, Determination of earthquake source parameters from waveform data for studies of global and regional seismicity, *J. Geophys. Res., 86*, 2825-2852, 1981.

Farina, F., E. Calais, C. DeMets, T. Dixon, P. Jansma, and P. Mann, GPS measurements across the northern Caribbean plate boundary zone: Preliminary results, *Eos Trans. AGU, 76* (17), Spring Meet. Suppl., S94, 1995.

Frankel, A., W. R. McCann, and A. J. Murphy, Observations from a seismic network in the Virgin Islands region: Tectonic structures and earthquake swarms, *J. Geophys. Res., 85*, 2669-2678, 1980.

Guzman-Speziale, M., W. D. Pennington, and T. Matumoto, The triple junction of the North America, Cocos, and Caribbean plates: Seismicity and tectonics, *Tectonics, 8*, 981-997, 1989.

Heubeck, C., and P. Mann, Geologic evaluation of plate kinematic models for the North American–Caribbean plate boundary zone, *Tectonophysics, 191*, 1-26, 1991.

Jany, I., K. M. Scanlon, and A. Mauffret, Geological interpretation of combined Seabeam, Gloria, and seismic data from Anegada Passage (Virgin Islands, North Caribbean), *Mar. Geophys. Res., 12*, 173-196, 1990.

Jordan, T. H., The present-day motions of the Caribbean plate, *J. Geophys. Res. 80*, 4433–4439, 1975.

Ladd, J. W., and J. S. Watkins, Active margin structures within the north slope of the Muertos trench, *Geol. Mijnbouw, 57*, 255–260, 1978.

Ladd, J. W., J. L. Worzel, and J. S. Watkins, Multifold seismic reflection records from the northern Venezuela basin and the north slope of the Muertos trench, in *Island Arcs, Deep Sea Trenches and Back Arc Basins*, edited by N. I. Talwani and W. C. Pitman, pp. 41-56, AGU, Washington D.C., 1977.

Ladd, J. W., T. C. Shih, and C. J. Tsai, Cenozoic tectonics of central Hispaniola and adjacent Caribbean Sea, *Am. Assoc. Petr. Geol. Bull., 65*, 466–489, 1981.

Langer, C. J., and G. A. Bollinger, Secondary faulting near the terminus of a seismogenic strike-slip fault: Aftershocks of the 1976 Guatemala earthquake, *Seismol. Soc. Am. Bull., 69*, 427-444, 1979.

Lundgren, P., F. Saucier, R. Palmer, and M. Langon, Alaska crustal deformation: Finite element modeling constrained by geologic and VLBI data, *J. Geophys. Res., 100*, 22,033-22,045, 1995.

MacDonald, W. D., Cretaceous-Tertiary evolution of the Caribbean, paper presented at 8th Caribbean Geology Conference, Saint Christophe, Curacao, 1976.

Mann, P., K. Burke, and T. Matumoto, Neotectonics of Hispaniola: Plate motion, sedimentation, and seismicity at a restraining bend, *Earth Planet. Sci. Lett., 70*, 311–324, 1984.

Mann, P., S. A. Tyburski, and E. Rosencrantz, Neogene development of the Swan Islands restraining-bend complex, Caribbean Sea, *Geology, 19*, 823–826, 1991.

Mann, P., F. W. Taylor, R. L. Edwards, and T-L. Ku, Actively evolving microplate formation by oblique collision and sideways motion along strike-slip faults: An example from the northeastern Caribbean plate margin, *Tectonophysics, 246*, 1-69, 1995.

Masson, D. G., and K. M. Scanlon, The neotectonic setting of Puerto Rico, *Geol. Soc. Am. Bull., 103*, 144-154, 1991.

McCann, W. R. and W. D. Pennington, Seismicity, large earthquakes, and the margin of the Caribbean plate, in *The Geology of North America*, vol. H, *The Caribbean Region*, edited by G. Dengo and J. E. Case, pp. 291–306, Geol. Soc. of Am., Boulder, Colo., 1990.

Melosh, H. J., and A. Raefsky, A simple and efficient method for introducing faults into finite element computations, *Seismol. Soc. Am. Bull., 71*, 1391-1400, 1981.

Melosh, H. J., and D. R. Williams, Mechanics of graben formation in crustal rocks: A finite element analysis, *J. Geophys. Res., 94*, 13,961-13,972, 1989.

Minster, B.J., and T.H. Jordan, Present-day plate motions, *J. Geophys. Res., 83*, 5331-5354, 1978.

Molnar, P., Gravity anomalies and the origin of the Puerto Rico Trench, *Geophys. J. R. Astron. Soc., 51*, 701-708, 1977.

Molnar, P., and L. R. Sykes, Tectonics of the Caribbean and Middle America regions from focal mechanisms and seismicity, *Geol. Soc. Am. Bull., 80*, 1639-1684, 1969.

Murphy, A. J., and W. R. McCann, Preliminary results from a new seismic network in the northeastern Caribbean, *Seismol. Soc. Am. Bull., 69*, 1497-1513, 1979.

Prentice, C. S., P. Mann, F. W. Taylor, G. Burr, and S. Valastro, Paleoseismicity of the North America–Caribbean plate boundary (Septentrional fault), Dominican Republic, *Geology, 21*, 49–52, 1993.

Rosencrantz, E., and P. Mann, SeaMARC II mapping of transform faults in the Cayman Trough, Caribbean Sea, *Geology, 19*, 690–693, 1991.

Rosencrantz, E., M. I. Ross, and J. G. Sclater, Age and spreading history of the Cayman trough as determined from depth, heat flow, and magnetic anomalies, *J. Geophys. Res., 93*, 2141–2157, 1988.

Russo, R. M., and A. Villaseñor, The 1946 Hispaniola earthquakes and the tectonics of the North America-Caribbean plate boundary zone, northeastern Hispaniola, *J. Geophys. Res., 100*, 6265-6280, 1995.

Saucier, F., and E. Humphreys, Horizontal crustal deformation in southern California from joint models of geologic and very long baseline interferometry measurements, in *Contributions of Space Geodesy to Geodynamics: Crustal Dynamics, Geodyn. Ser.*, vol. 23, edited by D. E. Smith and D. L. Turcotte, pp. 139-176, AGU, Washington, D.C., 1993.

Speed, R. C., and D. K. Larue, Extension and transtension in the plate boundary zone of the northeastern Caribbean, *Geophys. Res. Lett., 18*, 573–576, 1991.

Stein, S., J. Engeln, D. Wiens, K. Fujita, and R. Speed, Subduction seismicity and tectonics in the Lesser Antilles Arc, *J. Geophys. Res., 87*, 8642–8664, 1982.

Stein, S., C. DeMets, R. G. Gordon, J. Brodholt, D. Argus, J. F. Engeln, P. Lundgren, C. Stein, D. A. Wiens, and D. F. Woods, A test of alternative Caribbean plate relative motion models, *J. Geophys. Res., 93*, 3041–3050, 1988.

Sykes, L. R., W. R. McCann, and A. L. Kafka, Motion of the Caribbean Plate during the last 7 million years and implications for earlier Cenozoic movements, *J. Geophys. Res., 87*, 10,656–10,676, 1982.

Tomblin, J. F., The Lesser Antilles and Aves Ridge, in *Ocean Basins and Margins*, vol. 3, edited by A. E. M. Nairn and F. G. Stehli, pp. 467-500, Plenum, New York, 1975.

Zienkiewicz, O. C., and R. L. Taylor, *The Finite Element Method*, vol. 1, *Basic Formulation and Linear Problems*, 4th Ed., McGraw-Hill, New York, 1989.

P. R. Lundgren, Jet propulsion Laboratory, California Institute of Technology, 4800 Oak Grove Drive, MS 183-501, Pasadena, CA 91109-8099. (e-mail: paul@arrakis.jpl.nasa.gov)

R. M. Russo, Laboratoire de Tectonophysique, Université Montpellier II, Place Eugene Bataillon, 34095 Montpellier Cedex 05, France.

(Received March 31, 1995; revised November 29, 1995; accepted December 7, 1995.)